J Bio Tribo Corros (2017) 3:45
DOI 10.1007/s40735-017-0105-0

The Effect of Dissolved Oxygen in Slurry on Erosion–Corrosion of En30B Steel

Jiaren Jiang[1] · Yongsong Xie[1] · Md. Aminul Islam[1] · M. M. Stack[2]

Received: 15 March 2017 / Revised: 4 July 2017 / Accepted: 19 August 2017 / Published online: 29 August 2017
© Her Majesty the Queen in Right of Canada 2017

Abstract Synergistic effect between corrosion and wear has been widely recognized in many tribo-corrosion systems. In most wet application conditions, dissolved oxygen (DO) is a controlling factor to the dynamics of corrosion process and is therefore expected to have significant impact on the tribo-corrosion performance of materials. In this study, the effect of DO (0–24 ppm) on erosion–corrosion behaviour of En30B low-alloy steel has been investigated using a slurry pot erosion–corrosion test apparatus in a slurry containing 35 wt% silica sand and 3.5% NaCl solution at 30 and 45 °C. The synergistic effect and its contributing components, i.e. erosion-enhanced corrosion and corrosion-enhanced erosion, have been measured/analysed. The total erosion–corrosion loss and synergy of the En30B steel increases with DO in the slurry, initially rapidly at DO levels below ~5 ppm and then less rapidly at the higher DO levels. The synergistic effect is mainly due to corrosion-enhanced erosion with negligible contributions from erosion-enhanced corrosion. Temperature has a significant effect on the total erosion–corrosion loss. Total erosion–corrosion was 34% higher at 45 °C (in still air) than at 30 °C. Mechanisms for the observed phenomena have been discussed based on the concept of corrosion-accelerated micro-crack propagation.

✉ Jiaren Jiang
jiaren.jiang@nrc-cnrc.gc.ca

[1] Mining Wear and Corrosion Laboratory, National Research Council Canada, 4250 Wesbrook Mall, Vancouver, BC V6T 1W5, Canada

[2] Department of Mechanical Engineering, University of Strathclyde, 75 Montrose St, Glasgow G1 1XJ, UK

Keywords Slurry erosion–corrosion · Dissolved oxygen · Tribo-corrosion · Corrosion-enhanced erosion · Erosion–corrosion mechanism

1 Introduction

It has been well established that combined corrosion and erosion attacks can generate material loss that is much greater than the sum of losses caused by corrosion and erosion individually [1–11]. This phenomenon is commonly known as the synergistic effect or synergism. Such conditions are prevalent in the oil sands operations such as slurry pumps, slurry transport pipelines, and separation vessels. It has been recognized that erosion–corrosion constitutes an essential threat to the integrity of the oil sands slurry hydrotransport system [12]. Premature failure of the pipelines leads to considerable operation costs and could also bring disastrous impact on the environment. Obviously, knowledge of the relative magnitudes and interactions between the erosion and corrosion components of the total metal loss and the affecting factors is a prerequisite to the application of suitable control measures.

In oil sands operations, more than 90% of the pipelines are made of low-carbon steels [13] such as API X65 due to the comparatively low initial cost, although such steels have relatively poor corrosion and erosion resistance. A corrosive environment exists in these systems where the processing water contains high levels of chloride (typically 500 ppm or even higher) and other salts such as bicarbonate and sulphate originating from the ores. The slurry corrosivity is increased by the relatively high operating temperatures (40–60 °C) and pressures. Corrosion of slurry pipelines is generally controlled by dissolved oxygen (DO) in the slurry [14, 15]. That is, erosion–corrosion loss of the

pipeline will depend on the levels of DO in the slurry. According to Henry's law, dissolved oxygen in the slurry is proportional to the pressure applied to the slurry which decreases with increase in elevation (distance) of the pipe from the pump exit. It has indeed been observed that wear in oil sands hydrotransport pipelines decreases with pipe elevation and wear rate is much higher in the high-pressure system (2240–2600 kPa) than in the lower-pressure system (480–600 kPa) [16]. It was also noticed that wear patterns in the pipelines vary depending on the pipe length and elevation.

In the past two decades or so, extensive researches have been dedicated to the tribo-corrosion phenomena and remarkable progresses have been made in understanding the synergistic effect [7, 17–29]. Synergism in erosion–corrosion process can be attributed to two factors: (a) accelerated corrosion due to the co-existing mechanical damages by erosion (erosion-enhanced corrosion) and (b) increased erosion loss due to the presence of electrochemical corrosion (corrosion-enhanced erosion).

Mechanisms for erosion-enhanced corrosion have generally been attributed to the mechanical activation of the eroding surface due to

1. The striping or rupturing of corrosion films or preventing the formation of such films such that the underlying fresh metal surface is exposed and corrodes/repassivates rapidly following the exposure [14, 30, 31];
2. Increased ion/mass transportation by high turbulence levels due to the disruption of the solution boundary layer by impinging particles [15, 32–35]; or
3. Increased activity of the surface in the strain hardened layer due to the plastic deformation, rendering the metal more anodic and more susceptible to corrosion [36, 37].

Erosion-enhanced corrosion can be a result of one or all of the above reasons.

On the other hand, the corrosion-enhanced erosion process is far more complicated than erosion-enhanced corrosion. Several mechanisms/theories have been proposed each of which can be evoked to explain certain observed phenomena under given conditions. However, so far no one seems to be universally applicable.

1. Removal/dissolution of work-hardened surfaces by corrosion would expose the softer base metal and degrade the erosion resistance of the material [38].
2. Corrosion micro-pitting would increase the number of stress-concentrating defects or cause the roughening of the wear surface [39, 40], leading to more severe erosion loss.
3. In particulate reinforced wear resistant materials, preferential corrosion of the matrix or at the interface between the reinforcement hard phase and the matrix would weaken the matrix support to the hard particles and lead to premature loss of hard particles, resulting in significant corrosion-enhanced erosion [2, 41–43].
4. Anodic dissolution on the metal surface allows extra dislocation flux disappearing in the surface layer due to the so-called chemo-mechanical effect [44] and results in the softening of the eroding surface, degrading the erosion resistance of the material [7, 29, 45].
5. It was observed in erosion–corrosion test on stainless steels that platelets or lips formed during particle impingement were attacked/weakened by corrosion at their roots, making them more vulnerable to detachment by successive impingements [31]. This observation is similar to the mechanism proposed by Li et al. [46] which suggested that localized attack at disruptions in the surface oxide (caused by the particle impacts) enhances the rate of crack growth, causing the flakes to become detached and leading to a higher erosion rate.

Wood and Hutton [47] summarized some published erosion–corrosion testing data in the literature (including cavitation erosion and slurry erosion) and found that the ratio of synergy (S) to pure corrosion rate (C), S/C, could be related to the ratio of pure erosion rate (E) to pure corrosion rate, E/C, as follows.

(1) For results with medium S/C values, synergistic effects are approximately 30% of the total erosion rate

$$\frac{S}{C} = \exp\left[1.277 \ln\left(\frac{E}{C}\right) - 1.9125\right]$$

(2) For high S/C values, synergistic effects are more than 60% of the total erosion rate, resulting in a magnification of 2.5 or more,

$$\frac{S}{C} = \exp\left[0.075 \ln\left(\frac{E}{C}\right) + 1.222\right]$$

While these relationships may be useful for material selections in certain applications, they do not cast much significant insight into possible underlying mechanisms of erosion–corrosion.

Slurry pot erosion–corrosion assessment of different carbon steels (0.09C, 0.47C and 0.87C, respectively) at the authors' laboratory [48] showed that the erosion-only rates and synergistic levels generally decline with increasing carbon content and hardness [48]. As expected, the low-carbon steel pipe product displayed very mediocre erosion–corrosion resistance as a consequence of its very low

intrinsic corrosion resistance and inferior wear properties, although such steels are still being used as the dominant pipeline material. It is obviously beneficial to evaluate and search for alternative materials that may offer better erosion–corrosion resistance at similarly low capital cost.

Yu et al. [13] studied the effect of dissolved oxygen (0.016–3.26 ppm) on the erosion–corrosion behaviour of pipeline steel (X65) in aqueous slurries containing silica sand and CO_2 and found that dissolved oxygen (DO) considerably enhanced the CO_2 corrosion and the erosion–corrosion synergy. Tests were conducted in four types of environments: (1) open air (DO = 3.26 ppm), (2) N_2, (3) CO_2, and (4) $N_2 + CO_2$ mixture. Two DO levels were tested for the last three environments. At DO = 1.56 ppm, the highest erosion rate was observed when CO_2 was added for all the slurry velocities (3.5–8 m/s) while the lowest erosion rate was achieved when N_2 was passed to the slurry. When the level of DO was reduced to 0.016 ppm by blowing higher-pressure gases, erosion rate was the highest in open air (DO = 3.26 ppm) followed by testing in CO_2 with the lowest erosion rate in N_2, indicating the importance of DO in the corrosion and erosion–corrosion process of the pipe steel. Erosion surface examinations indicated that the surface eroded in the slurry with CO_2 at DO = 1.56 ppm had a lower hardness as compared with the surface eroded in air (DO = 3.26 ppm) and that eroded in CO_2 at DO = 0.016 ppm. Higher pitting density was also observed on eroded surface tested in slurry with CO_2 at DO = 1.56 ppm.

The objective of this paper is to investigate the effect of dissolved oxygen (DO) on the erosion–corrosion behaviour of an abrasion resistant AR 450 grade steel, En30B, at 30 and 45 °C in a 3.5% NaCl aqueous slurry. The work would provide valuable information for more effective control of erosion–corrosion of steel pipelines and other slurry handling equipment in oil sands and mining and mineral processing operations.

2 Experimental Details

2.1 Material and Specimen Preparation

Test specimens were prepared from quenched and tempered En30B steel plate. The steel hardness is 446HB. The nominal chemical compositions of the steel are as follows: C 0.26–0.34%, Ni 3.90–4.30%, Cr 1.10–1.40%, Mo 0.20–0.40%, Si 0.10–0.35%, Mn 0.40–0.60%, P 0.050% max, S 0.050% max, and Fe balance.

Specimen dimensions were 18 mm × 6 mm × 5 mm where 18 mm × 6 mm was the test surface which constituted a test surface area of 1.08 cm^2. All surfaces adjacent to the test surface were ground perpendicular to each other. The test surface was polished to a final surface finish obtained from a 1-μm diamond polishing paste. An electrical contact was attached to those specimens requiring electrochemical assessment/control. All specimens were subsequently mounted in epoxy to ensure that only the test surface was exposed to the prevailing conditions.

2.2 Test Equipment and Conditions

A slurry pot erosion–corrosion test system was used in this study. Details of the system have been provided in Refs. [41, 48]. The main components of the unit consist of a 4 L glass vessel, neoprene-lined impeller which is rotated to impel the slurry against the static test surfaces, heating/cooling system and a Gamry PC4/750 potentiostat for electrochemical and erosion–corrosion synergistic analysis.

The test conditions for erosion–corrosion assessment are shown in Table 1. Three DO levels were achieved by testing in air, bubbling through the slurry with pure N_2 or pure O_2 at a flow rate of 2 L/min (Porter Instrument B-250-3 flow meter). DO levels were measured using a HI 2400 DO Meter (Hanna Instruments) which has a reading accuracy of 0.01 ppm. Since the slurry almost 100% fills the slurry pot and is enclosed by the top cover, a positive pressure was always maintained due to the constant flowing of gas into the pot. This prevented ambient air being engulfed into the slurry pot during the test. As a result, the DO levels were maintained constant during the whole testing period after the very short initial stabilization time (rf. Fig. 1).

Distilled water was used for preparing the 3.5% NaCl solution used in making the slurries and was left in open air for at least 24 h before being used.

Temperature is an important factor affecting corrosion and also erosion–corrosion processes and deserves an in-depth investigation. In this work, two testing temperatures have been chosen to illustrate the general effect of slurry temperature. 45 °C is the most typical slurry temperature in the Canadian oil sands operations (tailings and hydrotransportation). Testing at 30 °C was conducted as a reference to examine the effect of temperature which can be most conveniently achieved on the testing equipment used in this study.

2.3 Methodology for Synergy Analysis

The erosion–corrosion synergy was determined/analysed according to the ASTM G119-04 standard guide [49]. The total material loss rate under erosion–corrosion (E–C) conditions, K_{ec}, can be related to the synergy, K_s, by the following equation

$$K_{ec} = K_{eo} + K_{co} + K_s \quad (1)$$

Table 1 Erosion–corrosion test conditions

Slurry composition	35 wt% AFS50–70 silica sand in 3.5 wt% NaCl solution
Slurry temperature (°C)	30, 45
Impeller speed (rpm)	900
Test duration (h)	6
Dissolved oxygen levels	Pure N_2 bubbling, air, pure O_2 bubbling

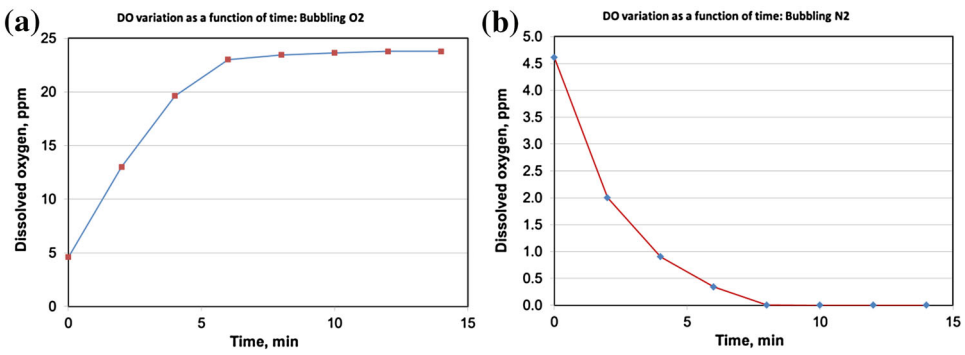

Fig. 1 Variation of dissolved oxygen (DO) in slurry as a function of time when bubbling **a** pure O_2 and **b** pure N_2 through the slurry

where K_{ec} = total erosion–corrosion rate, K_{eo} = erosion-only material loss rate (erosion in the absence of corrosion), K_{co} = corrosion-only material loss rate (corrosion in the absence of erosion), and K_s = synergy.

The total erosion–corrosion loss rate, K_{ec}, can also be divided into the various components as expressed in the following equation, Eq. (2):

$$K_{ec} = (K_{eo} + \Delta K_e) + (K_{co} + \Delta K_c) \quad (2)$$

The total erosion–corrosion rate, K_{ec}, was determined by measuring mass loss using a microbalance with a reading accuracy of 0.01 mg after testing in the prescribed erosion–corrosion conditions. The erosion-only loss rate, K_{eo}, was determined by measuring mass loss following erosion test in the same testing conditions with cathodic protection applied to the test specimen. The corrosion-enhanced erosion, ΔK_e, and erosion-enhanced corrosion, ΔK_c, were derived according to the following equations:

$$K_s = \Delta K_e + \Delta K_c = K_{ec} - (K_{eo} + K_{co}) \quad (3)$$

$$\Delta K_c = K_c - K_{co} \quad (4)$$

$$\Delta K_e = K_s - \Delta K_c \quad (5)$$

where K_s is the total synergy.

Total corrosion rate in the presence of erosion, K_c, and corrosion-only rate in the absence of erosion, K_{co}, were determined using polarization resistance technique. These were measured in the slurry pot erosion–corrosion test system with the rotator running with and without sand, respectively.

All the material loss rates were expressed in $cm^3/cm^2/h$.

Each data point reported in this paper is the average result of 2–4 repeats. Based on 5 repeated tests in air each conducted at 30 and 45 °C, respectively, the coefficient of variances for K_{ec} and K_{eo} ranged between 0.07 and 0.16, where coefficient of variance is defined as the ratio between the standard deviation and the average and is a measure of the repeatability of the testing results. Error bars drawn in the figures presented below represent the standard deviation of the data points.

3 Results

3.1 DO in the Slurry

In tests with pure O_2 or pure N_2 bubbling through the slurry, the variations of DO in the slurry as a function of time are shown in Fig. 1a, b, respectively. The measurements were conducted while the rotator/paddle was running. The levels of DO in the slurry reached dynamic equilibrium within less than bout 8 min. This very short transit time as compared with the total test time of 6 h is not expected to significantly affect the testing results.

The equilibrium levels of DO in the slurry reached under different testing conditions are provided in Table 2.

Table 2 Dissolved oxygen (DO) levels in slurry under the different test conditions

Environment	Temperature (°C)	Dissolved O_2 (ppm)
Bubbling pure O_2	45	23.78
Air	45	4.61
Bubbling pure N_2	45	0.00
Air	30	6.38

3.2 Synergistic Effect Analysis and Effects of DO and Temperature

Experimental results for the variation of total erosion–corrosion loss rate, K_{ec}, and its various components according to Eq. (1) (K_s, K_{eo}, and K_{co}) are shown in Fig. 2 as a function of DO levels.

At the testing temperature of 45 °C, both the total erosion–corrosion loss rate, K_{ec}, and the synergy, K_s, increased rapidly with increasing DO at low DO levels below about 5 ppm and then increased less rapidly at the higher DO values. The corrosion-only loss rate, K_{co}, showed similar trend as K_{ec} and K_s; however, it accounted for only a very small fraction of the total erosion–corrosion loss rate. On the other hand, the erosion-only loss rate, K_{eo}, was almost the same under all the testing conditions, with a very slight increase with increase in DO. Nevertheless, the difference of K_{eo} in the different environments (DO levels) is less than 10% of the average value and is thus within the testing error range. Test result at 30 °C in open air for K_{eo} was close to that at 45 °C, which is expected because such small temperature difference should have little effect on pure mechanical erosion damage for steels.

The cathodic potential and cathodic current applied during the measurement of the erosion-only loss rate, K_{eo}, in the various environments and temperatures are shown in Table 3. It is apparent that very little cathodic current is required when tested in the N_2 bubbling conditions to suppress corrosion while the cathodic current is very similar for testing in open air and in bubbling O_2 environment.

The total material loss rate, K_{ec}, the corrosion loss rate, K_{co}, and the synergistic effect, K_s, at 30 °C were considerably lower than those at 45 °C (Fig. 2).

Under all the testing conditions, synergy accounted for a very high fraction of the total erosion–corrosion loss. The effect of DO on the relative contribution of synergy to the total erosion–corrosion rate, K_s/K_{ec}, is shown in Fig. 3. Similarly to the variation of total erosion–corrosion and total synergy as a function of DO levels, the relative contribution of synergy also increased with increase in DO levels first rapidly at low DO levels (below ~5 ppm) and then at slower rate at the higher DO levels. The relative contribution of synergy was slightly lower at 30 °C than at 45 °C.

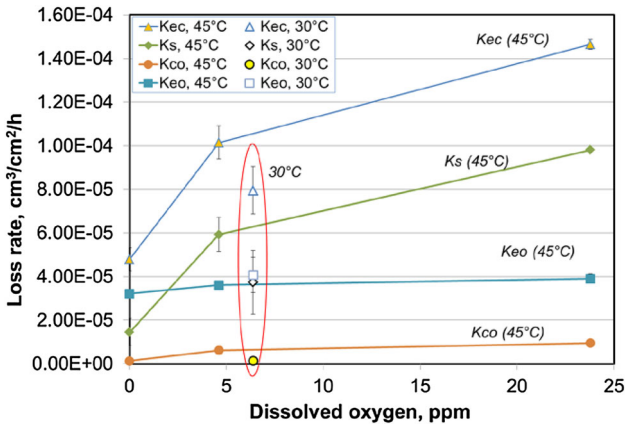

Fig. 2 Effect of dissolved oxygen (DO) on total erosion–corrosion and the synergistic effect

According to Eq. (2), more detailed analysis was conducted for the contributions of various components of synergy. The results are shown in Fig. 4. Clearly, the total synergy, K_s, was dominated by corrosion-enhanced erosion, ΔK_e, while the contribution of erosion-enhanced corrosion, ΔK_c, was very small. This is in line with most of our previous observations on many industrial materials. The relative contribution of erosion-enhanced corrosion at 30 °C was much smaller than that at 45 °C.

The corrosion rate of steels in salt solutions is usually controlled by dissolved oxygen. This is clearly demonstrated by the results shown in Fig. 5. The material loss rate of total corrosion in the presence of erosion, K_c, and the corrosion-only loss rate, K_{co}, both increased rapidly with increase in the concentration of DO at the low DO levels and then increased much more slowly at DO levels greater than ~5 ppm.

As expected, temperature had very significant effect on the corrosion rates, K_c and K_{co}.

4 Discussion

4.1 The Influence of DO

From testing results at 45 °C, the total erosion–corrosion rate and all the components of synergy except for the erosion-only rate followed the similar trend as a function of DO level, i.e. the material loss rate increased rapidly with increase in DO at low DO levels (below 5 ppm from the limited number of investigated DO levels) and then increased less rapidly at the higher DO levels. The similar phenomenon was observed by Cooke et al. [50] when studying the erosion–corrosion of a carbon steel using a toroidal type erosion tester in fine gold tailings slurry; their results are shown in Fig. 6.

As reviewed in the Introduction, in spite of the extensive efforts, so far the synergistic phenomena in erosion–corrosion and more broadly in tribo-corrosion are not well understood yet. In many cases, corrosion during erosion–corrosion test only accounts for a very small fraction of the total material loss (e.g. Figs. 2, 4). However, the presence of corrosion can lead to significant synergistic material loss as has been observed in this study. In Fig. 7, the total erosion–corrosion loss rate, K_{ec}, synergy, K_s, and

Table 3 Cathodic protection conditions for measuring the erosion-only loss rate, K_{eo}

Temperature (°C)	Environment	Cathodic potential (mV)	Cathodic current (mA)
30	Air	−782 to −785	−2.4 to −2.6
45	N_2	−893 to −897	−0.08 to −0.15
45	Air	−708 to −782	−2.5 to −5.0
45	O_2	−785	−2.5 to −7.0

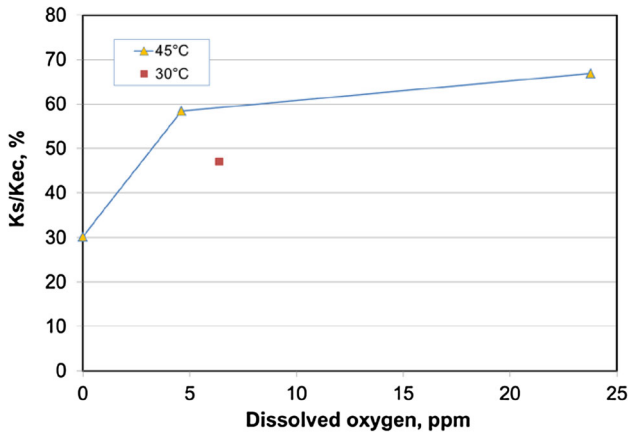

Fig. 3 Relative contribution of synergy to the total erosion–corrosion loss rate, K_s/K_{ec}, as a function of dissolved oxygen (DO) levels

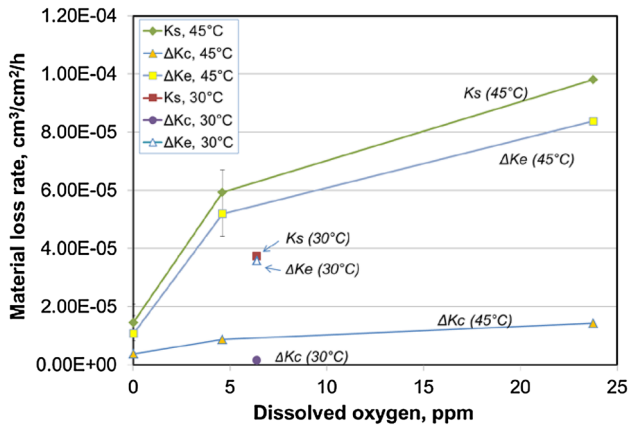

Fig. 4 Effect of dissolved oxygen (DO) on the various components of synergy, K_s, erosion-enhanced corrosion, ΔK_c and corrosion-enhanced erosion, ΔK_e

components of synergy, ΔK_e and ΔK_c, are plotted against the total corrosion rate, K_c, under erosion–corrosion conditions. Almost a linear relationship is seen for all these material loss components. This suggests that the synergistic effect is controlled by or closely related to the corrosion behaviour of the metal under the given erosion–corrosion conditions and, more specifically, by corrosion activities on the erosion surface. Thus, to understand the effect of DO on the erosion–corrosion behaviour of the En30B steel (Figs. 2, 3, 4), it is important to first understand the variation of corrosion rate as a function of DO levels in the slurry (Fig. 5).

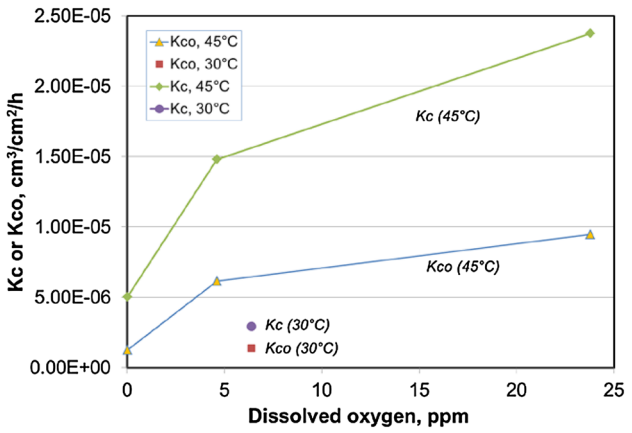

Fig. 5 Effect of dissolved oxygen (DO) on the total corrosion loss rate, K_c, and the corrosion-only rate, K_{co}

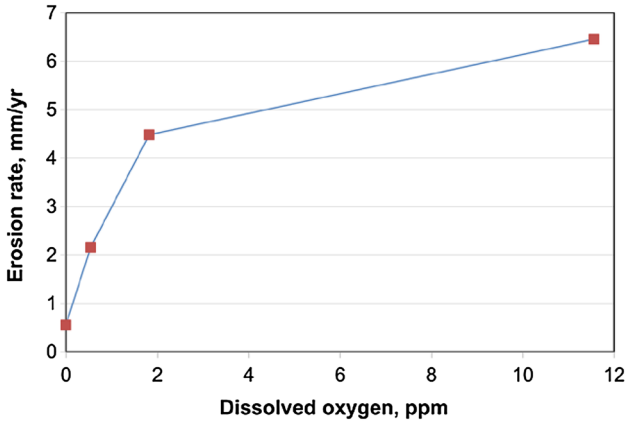

Fig. 6 Erosion rate of carbon steel versus dissolved oxygen (DO) in a fine gold tailings slurry [50]

Corrosion of steels in (near neutral) NaCl solutions is a complicated process but the half-cell anodic and cathodic reactions can generally be described by the following Eqs. (6) and (7), respectively:

$$\mathrm{Fe} = \mathrm{Fe}^{2+} + 2\mathrm{e}^- \tag{6}$$

$$\frac{1}{2}\mathrm{O}_2 + \mathrm{H}_2\mathrm{O} + 2\mathrm{e}^- = 2\mathrm{OH}^- \tag{7}$$

The corrosion rate is usually controlled by the availability of oxygen on the metal surface, i.e. the diffusion limiting current density, i_L. Figure 8a schematically illustrates the (half-cell) polarization curves for cathodic

oxygen reduction reaction [Eq. (7)] at different DO levels from C_1 to C_8. At a given DO level, the corrosion current, $i_{corr(k)}$ ($k = 1$–8), is determined by the intersection of the corresponding cathodic polarization curve and the anodic iron oxidation (half-cell) polarization curve [Eq. (6)]. Thus, at relatively low DO levels (below C_3 in the illustration Fig. 8a), the corrosion current density, $i_{corr(k)}$, is determined by the limiting current density, $i_{L(k)}$, which is proportional to the DO concentration and increases rapidly with increase in DO levels. However, when the DO concentration exceeds certain level (the transition DO level), the corrosion current density, i_{corr}, is lower than the limiting current density, i.e. the corrosion process starts to be controlled by both the cathodic (oxygen reduction) activation and the anodic (iron oxidation) reaction rates. The increase in corrosion rate becomes less and less rapidly with increase in DO levels. Thus, the dependence of corrosion current density with DO levels can be schematically depicted by Fig. 8b which qualitatively explains the observed effect of DO on corrosion of the steel, Fig. 5.

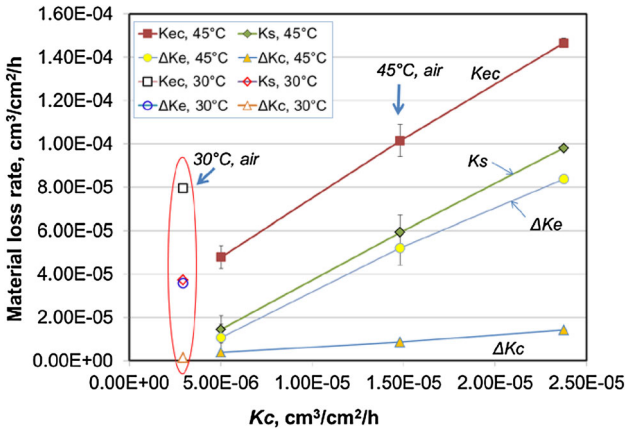

Fig. 7 Correlation of total erosion–corrosion (K_{ec}) and synergistic effect (ΔK_e, ΔK_c) with the total corrosion rate (K_c) during erosion–corrosion

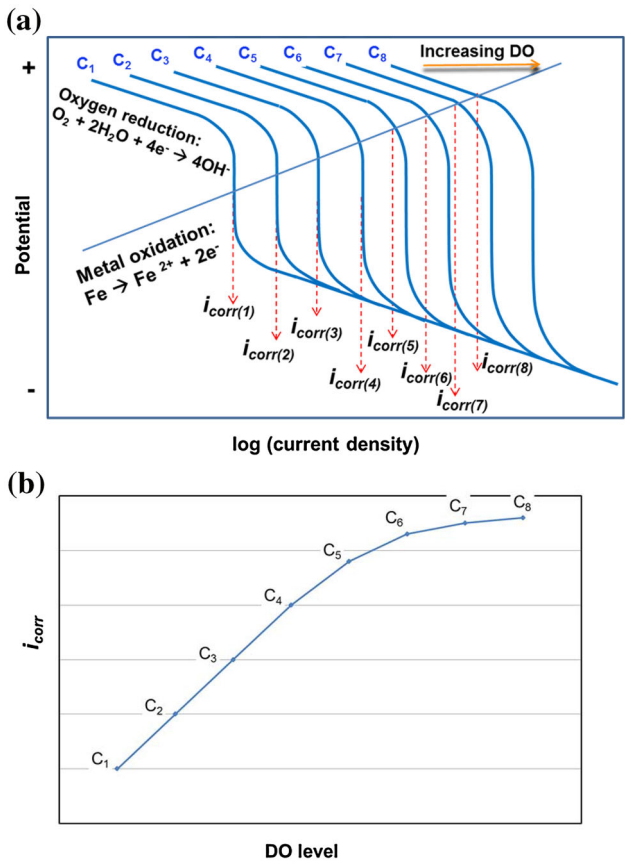

Fig. 8 **a** Schematic representation of the influence of dissolved oxygen (DO) on corrosion current density (corrosion rate) of iron as the intersection of a DO-dependent (diffusion limiting current density) cathodic polarization curve with the anodic polarization curve. **b** The resulting dependence of corrosion current density, i_{corr}, on DO levels

4.2 On the Mechanisms of Corrosion-Enhanced Erosion

Figure 3 shows that synergy can account for 30% to almost 70% of the total erosion–corrosion loss. The total synergy is dominated by corrosion-enhanced erosion with only a very small contribution from erosion-enhanced corrosion (Fig. 4).

The erosion-enhanced corrosion phenomenon observed for En30B steel in this study can be reasonably attributed to the mechanical activation of the erosion surface (by creating fresh metal surfaces and increasing density of defects in the surface layer). This view point can be supported by the almost linear relationship between the total corrosion rate during erosion–corrosion test, K_c, and pure corrosion rate in the absence of erosion, K_{co}, as displayed in Fig. 9. Under all the testing conditions, the pure erosion rate was at almost the same level (Fig. 2) and thus new surfaces

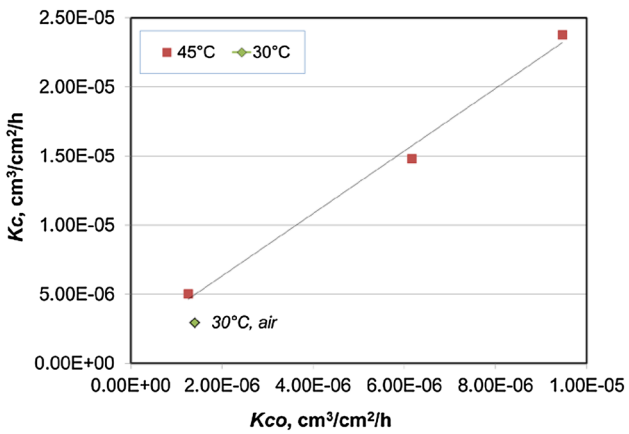

Fig. 9 Relationship between total corrosion rate, K_c, and corrosion-only rate, K_{co}

(area and activities) exposed would be expected to be almost the same. The total corrosion loss is thus expected to be controlled by, and proportional to, the corrosion resistance of the steel (K_{co}).

On the other hand, the significant contribution of corrosion-enhanced erosion to synergy can be explained as follows.

Jiang et al. [25, 28] propose a generic model to describe the synergistic effect in tribo-corrosion. They argued that the generation of wear debris (in any wear or erosion process) can essentially be regarded as a low-cycle fatigue process which involves the micro-crack initiation and propagation. Micro-cutting is the limiting case of low-cycle fatigue where the fatigue life is equal to 1 cycle. When wear occurs in the presence of "reactive species" either in dry or in wet environments that weakens the atomic bonding at the crack tip, the micro-crack propagation rate is accelerated and a positive synergistic effect is expected. This concept of micro-crack propagation can be broadened to include localized corrosion attacks that accelerate the formation of wear debris by successive wear actions. For example, Rajahram et al. [31] observed in erosion–corrosion study of stainless steels that platelets or lips formed during particle impingement were attacked by corrosion at their roots, making them easier to be detached by successive impingements.

Gutman [44] described and theoretically proved the phenomenon that the mobility of dislocations in near the solid surface increases and the surface hardness and flow stress of materials decrease with increasing anodic dissolution current density. According to Gutman [44], the weakening of inter-atomic bonds as a result of dissolution of surface layer results in softening of crystals. The chemical potential gradient from the surface layer to the bulk of the solid material is likely to result in an additional dislocation flux with the dislocation moving to the surface layer, enhancing localized surface plastic deformation. Surface softening of steels under applied anodic current was also experimentally observed by Lu et al. [45] which was directly attributed to the corrosion-enhanced erosion of carbon steels by assuming a direct/linear correlation between erosion and hardness [29, 45].

Because the mean free path of dislocation has a limited value, only dislocations situated in the surface layer region within a depth of the mean free path can reach the surface. Therefore, it is expected that the chemo-mechanical effect can only affect the mechanical properties in this very thin surface layer and may not be able to account for the very significant increase of erosion due to corrosion (the corrosion-enhanced erosion).

By considering the chemo-mechanical softening effect of corrosion current, the low-cycle micro-fatigue model of corrosion-enhanced erosion by Jiang et al. [25, 28] can be extended to explain the observation that small increase in corrosion rate has led to significant accelerated erosion. Thus, bonds in the tip region of a micro-crack can be markedly weakened due to the chemo-mechanical softening under the influence of anodic current, causing more rapid propagation of the crack. According to this model, weakening of only the bonds in the very crack tip region is necessary in order to achieve significantly accelerated erosion rate.

Based on the above argument, in the current study, the increase in corrosion rate with DO levels can be expected to cause increased softening effect at micro-crack tips and/or roots of plastically deformed lips, accelerate the formation of wear debris and therefore lead to more significant corrosion-enhanced erosion and total synergy, as is shown by Fig. 7.

5 Conclusions

The effect of dissolved oxygen (DO) in the range of 0–24 ppm on erosion–corrosion behaviour of En30B low-alloy steel has been investigated using a slurry pot erosion–corrosion test apparatus in a slurry containing 35 wt% silica sand and 3.5% NaCl solution at 30 and 45 °C. The following observations have been made.

1. The total erosion–corrosion loss rate, the synergy and its various components (erosion-enhanced corrosion and corrosion-enhanced erosion) of the En30B steel all increase with DO in the slurry, initially rapidly at DO levels below $\sim$5 ppm and then much less rapidly at the higher DO levels.
2. The synergistic effect is mainly due to corrosion-enhanced erosion with negligible contributions from erosion-enhanced corrosion.
3. The total erosion–corrosion loss rate and synergy are much higher at 45 °C (in air) than at 30 °C.
4. Mechanisms for corrosion-enhanced erosion have been discussed based on the low-cycle fatigue model of erosion invoking the concept of chemo-mechanical softening effect in the micro-crack tip region under the influence of anodic corrosion current. However, further experimental evidences are required to confirm such mechanisms.

Acknowledgements The authors would like to acknowledge members of the NRC/Industry Mining Wear Materials Consortium for their support and sponsorship of this work and express their thanks to Baisheng (Peter) Yao at the Mining Wear and Corrosion Lab for his technical assistance in conducting the experimental work.

Compliance with Ethical Standards

Conflict of interest On behalf of all authors, the corresponding author states that there is no conflict of interest.

References

1. Neville A, Reza F, Chiovelli S, Revega T (2005) Erosion–corrosion behavior of WC based MMCs in liquid–solid slurries. Wear 259:181–195
2. Reyes M, Neville A (2001) Mechanisms of erosion–corrosion on a cobalt-base alloy and stainless-steel UNS S17400 in aggressive slurries. J Mater Eng Perform 10:723–730
3. Zhang T, Luo Y, Li DY (1999) Modification of aluminide coating with yttrium for improved resistance to corrosive erosion. J Mater Eng Perform 8:635–640
4. Grewal HS, Agrawal A, Singh H (2013) Design and development of high-velocity slurry erosion test rig using CFD. J Mater Eng Perform 22:152–161
5. Souza VAD, Neville A (2007) Aspects of microstructure on the synergy and overall material loss of thermal spray coatings in erosion–corrosion environments. Wear 263:339–348
6. Hussain EAM, Robinson MJ (2007) Erosion–corrosion of 2205 duplex stainless steel in flowing seawater containing sand particles. Corros Sci 49:1737–1744
7. Barik RC, Wharton JA, Wood RJK, Stokes KR (2009) Electromechanical interactions during erosion–corrosion. Wear 267: 1900–1908
8. Neville A, Reyes M, Hodgkiess T, Gledhill A (2000) Mechanisms of wear on a Co-base alloy in liquid–solid slurries. Wear 238:138–150
9. Neville A, Hodgkiess T (1999) Characterisation of high-grade alloy behaviour in severe erosion–corrosion conditions. Wear 233–235:596–607
10. Neville A, Hodgkiess T, Xu H (1999) An electrochemical and microstructural assessment of erosion–corrosion of cast-iron. Wear 233–235:523–534
11. Clark HM (1993) The influence of flow field in slurry erosion. Wear 152:223–240
12. Tian BR, Cheng YF (2006) Erosion–corrosion of hydrotransport pipes in oil sand slurries. Bull Electrochem 22:329–335
13. Yu B, Li DY, Grondin A (2013) Effects of the dissolved oxygen and slurry velocity on erosion–corrosion of carbon steel in aqueous slurries with carbon dioxide and silica sand. Wear 302:1609–1614
14. Postlethwaite J, Dobbin MH, Bergevin K (1986) The role of oxygen mass transfer in the erosion–corrosion of slurry pipelines. Corrosion 42:514–521
15. Postlethwaite J, Lotz U (1988) Mass transfer at erosion–corrosion roughened surfaces. Can J Chem Eng 66:75–78
16. Parent LL, Li DY (2013) Wear of hydrotransport lines in Athabasca oil sands. Wear 301:477–482
17. Yang Y, Cheng YF (2012) Parametric effects on the erosion–corrosion rate and mechanism of carbon steel pipes in oil sands slurry. Wear 276–277:141–148
18. Rajahram SS, Harvey TJ, Wood RJK (2009) Erosion–corrosion resistance of engineering materials in various test conditions. Wear 267:244–254
19. Burstein GT, Sasaki K (2000) Effect of impact angle on slurry erosion–corrosion of 304 L stainless steel. Wear 240: 80–94
20. Jana BD, Stack MM (2005) Modelling impact angle effects on erosion–corrosion of pure metals: construction of materials performance maps. Wear 259:243–255
21. Abbade NP, Crnkovic SJ (2000) Sand–water slurry erosion of API 5L X65 pipe steel as quenched from intercritical temperature. Tribol Int 33:811–816
22. Meng H, Hu X, Neville A (2007) A systematic erosion–corrosion study of two stainless steels in marine conditions via experimental design. Wear 263:355–362
23. Mischler S, Debaud S, Landolt D (1998) Wear-accelerated corrosion of passive metals in tribocorrosion systems. J Electrochem Soc 145:750–758
24. Jemmely P, Mischler S, Landolt D (2000) Electrochemical modeling of passivation phenomena in tribocorrosion. Wear 237:63–76
25. Jiang J, Stack MM (2006) Modelling sliding wear: from dry to wet environments. Wear 261:954–965
26. García I, Drees D, Celis JP (2001) Corrosion-wear of passivating materials in sliding contacts based on a concept of active wear track area. Wear 249:452–460
27. Landolt D, Mischler S, Stemp M, Barril S (2004) Third body effects and material fluxes in tribocorrosion systems involving a sliding contact. Wear 256:517–524
28. Jiang J, Stack MM, Neville A (2002) Modelling the tribo-corrosion interaction in aqueous sliding conditions. Tribol Int 35:669–679
29. Guo HX, Lu BT, Luo JL (2005) Interaction of mechanical and electrochemical factors in erosion–corrosion of carbon steel. Electrochim Acta 51:315–323
30. Xu J, Zhuo C, Tao J, Jiang S, Liu L (2009) Improving the corrosion wear resistance of AISI 316L stainless steels by particulate reinforced Ni matrix composite alloying layer. J Phys D Appl Phys 42:1–12
31. Rajahram SS, Harvey TJ, Wood RJK (2011) Electrochemical investigation of erosion–corrosion using a slurry pot erosion tester. Tribol Int 44:232–240
32. Clark HM, Hartwich RB (2001) A re-examination of the 'particle size' effect in slurry erosion. Wear 248:147–161
33. Harvey TJ, Wharton JA, Wood RJK (2007) Development of a synergy model for erosion–corrosion of carbon steel in a slurry pot. Tribol Mater Surf Interfaces 1:33–47
34. Postlethwaite J, Holdner DN (1975) Wall mass transfer in horizontal slurry pipelines. Can J Chem Eng 53:31–35
35. Postlethwaite J, Holdner DN (1976) Wall mass transfer in vertical and horizontal slurry pipelines. Can J Chem Eng 54:255–258
36. Oltra R, Chapey B, Renaud L (1995) Abrasion–corrosion studies of passive stainless steels in acidic media: combination of acoustic emission and electrochemical techniques. Wear 186–187:533–541
37. Li W, Li DY (2005) Variations of work function and corrosion behaviour of deformed copper surfaces. Appl Surf Sci 240:388–395
38. Matsumura M, Oka Y, Hiura H, Yano M (1991) The role of passivating film in preventing slurry erosion–corrosion of austenitic stainless steel. ISIJ Int 31:168–172
39. Postlethwaite J, Brady BJ, Hawrylak MW, Tinker EB (1978) Effects of corrosion on the wear patterns in horizontal slurry pipelines. Corrosion 34:245–250
40. Postlethwaite J (1981) Effect of chromate inhibitor on the mechanical and electrochemical components of erosion–corrosion in aqueous slurries of sand. Corrosion 37:1–5
41. Jones M, Waag U (2011) The influence of carbide dissolution on the erosion–corrosion properties of cast tungsten carbide/Ni-based PTAW overlays. Wear 271:1314–1324
42. Bester JA, Ball A (1993) The performance of aluminium alloys and particulate reinforced aluminium metal matrix composites in erosive-corrosive slurry environments. Wear 162–164:57–63
43. Zheng Yugui, Yao Zhiming, Wei Xiangyun, Ke Wei (1995) The synergistic effect between erosion and corrosion in acidic slurry medium. Wear 186–187:555–561
44. Gutman EM (1998) Mechanochemistry of materials. Cambridge International Science Publishing, Cambridge
45. BT Lu, JL Luo, JF Lu (2004) Chemo-mechanical effect in erosion–corrosion process of carbon steel. Corrosion, Paper 04659

46. Li Y, Burstein T, Hutchings IM (1995) The influence of corrosion on the erosion of aluminium by aqueous silica slurries. Wear 186–187:515–522
47. Wood RJK, Hutton SP (1990) The synergistic effect of erosion and corrosion: trends in published results. Wear 140:387–394
48. Jones M, Llewellyn RJ (2009) Erosion–corrosion assessment of materials for use in the resources industry. Wear 267:2003–2009
49. ASTM G119 - 09 (2009) Standard guide for determining synergism between wear and corrosion. ASTM International, West Conshohocken. doi:10.1520/G0119-09
50. R Cooke, G Johnson, P Goosen (2000) Laboratory apparatus for evaluating slurry pipeline wear. In: SAIT Seminar, Economics of Wear Materials, 13 Mar 2000